Ocean Sci. Discuss., 10, 2461–2479, 2013
www.ocean-sci-discuss.net/10/2461/2013/
doi:10.5194/osd-10-2461-2013

Ocean Science
Discussions
Open Access

Reconciling the north–south density difference scaling for the Meridional Overturning Circulation strength with geostrophy

A. A. Cimatoribus[1,*], **S. Drijfhout**[2,1], **and H. A. Dijkstra**[3]

[1]Global Climate Division, Royal Netherlands Meteorological Institute, De Bilt, the Netherlands
[2]National Oceanography Centre, Southampton, UK
[3]Institute for Marine and Atmospheric research Utrecht, Utrecht University, Utrecht, the Netherlands
[*]now at: Department of Physical Oceanography, Royal Netherlands Institute for Sea Research, Den Burg, the Netherlands

Received: 27 November 2013 – Accepted: 9 December 2013 – Published: 20 December 2013

Correspondence to: A. A. Cimatoribus (andrea.cimatoribus@nioz.nl)

Published by Copernicus Publications on behalf of the European Geosciences Union.

Abstract

Since the formulation of the Stommel two-box model for the meridional overturning circulation (MOC), various theoretical and conceptual models for the MOC emerged based on scaling the MOC strength with the north south density difference. At the same time the MOC should obey geostrophic balance with an east-west density difference. Scaling with the north south density gradient seems to violate the common assumption of geostrophic balance for the large-scale circulation, which implies that the pressure gradient is orthogonal to the flow. In this brief report, we report on the results of a series of numerical simulations in an idealized ocean basin (with a zonally periodic channel at its southern end). The simulations performed with different surface forcing conditions indicate that the meridional and zonal density gradients, important for the MOC strength, are in fact related to each other through the stratification located at the northern end of the periodic channel. The results suggest that the water properties at the northern end of the periodic channel play a crucial role in setting the MOC strength, possibly explaining the sensitivity of climate models to the conditions in this area.

1 Introduction

In the classical view inspired by Stommel (1961), the Meridional Overturning Circulation (MOC) can be considered as an example of "horizontal convection" (two dimensional overturning with low aspect ratio) in a non-rotating fluid. In this view, the MOC strength measured by the MOC streamfunction maximum (Ψ) satisfies a power-law relation with the applied surface buoyancy restoring (Hughes and Griffiths, 2008; Den Toom and Dijkstra, 2011).

With rotational effects included, the thermal wind relation $\partial v/\partial z = (1/f)\partial b/\partial x$ is essential for diagnosing the MOC strength, with v being meridional velocity, f being the Coriolis parameter and b the buoyancy. Thermal wind balance has been used to

OSD
10, 2461–2479, 2013

obtain a scaling between MOC strength and vertical diffusivity (e.g. Park and Bryan, 2000; Marotzke, 1997; Dijkstra, 2008, and references therein). Thermal wind balance underlies the scaling used in Gnanadesikan (1999) and Johnson et al. (2007), and derived for a two-layer model in Johnson and Marshall (2002) as:

$$\Psi \sim \frac{1}{f} \Delta b_z D_E^2. \quad (1)$$

Here, Δb_z is the buoyancy difference between the upper and lower branches of the MOC and D_E is the pycnocline depth at the eastern boundary, at the same latitude where the pycnocline outcrops in the western boundary (see sketch in Fig. 1).

For a closed basin extending over one hemisphere, various authors noted that the overturning rate would scale as (e.g. Marotzke, 1997):

$$\Psi \sim \frac{1}{f} \Delta b_{TP} D^2, \quad (2)$$

where D represents the pycnocline depth, set in Marotzke (1997) by an advective–diffusive balance. The buoyancy difference Δb_{TP} is measured at the surface, between the tropical and polar ends of the basin considered. The implicit assumption of this scaling is that the zonal and meridional velocity scales are linearly related (Park and Bryan, 2000), allowing to use meridional instead of zonal buoyancy gradient. The meridional gradient is, in turn, largely set by the surface boundary conditions for buoyancy (Stommel, 1961; Thorpe et al., 2001; Wang et al., 2010).

The extension of the scaling based on meridional density difference to an inter–hemispheric overturning circulation is not straightforward but is supported by the numerical results of Marotzke and Klinger (2000), Weijer et al. (2002) and Levermann and Fürst (2010), who consider the correlation between MOC strength and meridional buoyancy gradient. De Boer et al. (2010) discussed the limits of this approach, finding that the depth scale that should be used in the scaling is the depth of Ψ, rather than the pycnocline depth.

OSD
10, 2461–2479, 2013

On physical grounds, a scaling based on the meridional buoyancy gradient suggests that a meridional pressure gradient is driving a circulation on the meridional plane. Such a mechanism can function only in the western boundary, where geostrophy can be overcome, and velocity can be aligned to the pressure gradient (Weijer et al., 2002; Griesel and Maqueda, 2006; Marshall and Pillar, 2011; Sijp et al., 2012; Tailleux, 2013).

Even if the MOC is driven by meridional pressure gradients in the western boundary, it must still be in geostrophic balance on the basin scale. The thermal wind relationship should give a valid scaling:

$$\Psi \sim \frac{1}{f} \Delta b_{\mathrm{EW}} h^2, \tag{3}$$

where Δb_{EW} is the buoyancy difference between the eastern and the western boundary, and h is a depth scale. Both are measured at the latitude of Ψ. Numerical and observational evidence shows that the geostrophic balance is a good diagnostic of the large-scale motions of the ocean in general, and of the MOC in particular (e.g. Hautala et al., 1994; Marotzke and Klinger, 2000; Cunningham et al., 2007; Cessi and Wolfe, 2009; Wunsch, 2011).

Here, we try to justify the use of a north–south scaling for a flow in geostrophic balance. We will do so by demonstrating that a suited north–south buoyancy difference scales with the east–west buoyancy difference where the MOC is maximum. In particular, we will discuss the scaling:

$$\Psi \sim \frac{1}{f} \Delta b_{\mathrm{SN}} h^2, \tag{4}$$

where the relevant buoyancy difference is assumed to be the one between the region at the northern end (Ne) of the Antarctic Circumpolar Current (ACC), where Antarctic Intermediate Water forms, and the dense water formation regions in the North Atlantic. In Sect. 2 our hypothesis is presented in detail, in Sect. 3 the numerical model used is described, Sects. 4 and 5 present and discuss the results.

OSD
10, 2461–2479, 2013

2 Scaling of the AMOC with north–south density difference

The upper ocean (generically referred to as the pycnocline) has a relatively high buoyancy frequency. The deeper ocean is instead filled with less stratified, denser water formed in the subpolar regions. The isopycnal surface defined by the stratification maximum, separating the pycnocline from the deeper ocean, slopes down to the east at the latitudes where the subtropical and subpolar gyres meet in the Northern Hemisphere (NH) (at θ_b in Fig. 2). The pycnocline shoals in the west while the southward flowing western boundary current sinks below it. We expect Ψ to be determined by the strong buoyancy difference across the pycnocline, projected in the zonal direction at θ_b. If this is the case, Ψ is in thermal wind balance with the buoyancy difference between the lower pycnocline in the east, and the upper deep western boundary current in the west (Fig. 2).

A link between Δb_{EW} and Δb_{SN} can be made by considering the pycnocline structure in a basin with a periodic channel at its southern end (Se). In the Southern Hemisphere (SH), the outcropping latitude of the pycnocline tends to be locked at the northern end (Ne) of the periodic channel (Vallis, 2000). This outcropping latitude is marked in Fig. 2 by θ_{O} (in the real ocean, the Antarctic Intermediate Water formation regions). Basin–scale gyre circulation in the enclosed basin flattens the isopycnals more efficiently than eddies in the zonally periodic channel, where no geostrophic meridional flow can be supported. This different mapping of surface buoyancy onto vertical stratification, in the zonally enclosed basin and in the zonally periodic channel, is reflected on the lower buoyancy frequency of the water classes outcropping south of θ_{O}. The density class outcropping at the Ne of the periodic channel is thus a natural choice for the lower boundary of the pycnocline, since this isopycnal separates waters with different stratification. This is true even in presence of finite vertical diffusivity, as long as stratification does not become completely dominated by diabatic effects (Vallis, 2000).

Here we hypothesize that the highest buoyancy entering the scaling (Eq. 3), i.e. b_{E}, is in fact set in the SH, by the lightest water upwelling at the Ne of the periodic channel,

OSD
10, 2461–2479, 2013

or can at least be identified by measuring buoyancy in this region (so $b_E \sim b_S$). Assuming that diffusive upwelling is not a first order component of the circulation in the Atlantic ocean (Talley, 2013), any change of b_S will be reflected on b_E; the density classes between b_S and b_E would have to upwell diffusively within the Atlantic basin, and thus cannot be part of the MOC's lower branch. The mechanism through which anomalies propagate from South to North is most likely connected to the one described by Marshall and Johnson (2013) in a two layer model, involving Rossby waves travelling around the basin. On the other hand, the lowest buoyancy involved in the scaling (Eq. 3), b_W, is limited by the dense water formation in the NH, and thus $b_W \sim b_N$, their difference being due to mixing of newly formed dense water with other water masses (a process which we cannot expect to represent realistically in this model).

3 Methods

The hypothesis discussed in the previous section was tested with a set of numerical experiments. With this aim, a model of an interhemispheric basin centered at the equator was set up using the MITgcm (Marshall et al., 1997). The domain extends over 60° in longitude, 135° in latitude and has a constant depth of 4500 m. A zonally periodic channel with a 3000 m deep sill, 16° wide in the meridional direction, is added at the basin's Se. The model resolution is 1.35° in the meridional direction and 1.5° in the zonal direction. In the vertical, 20 layers are used with cell thickness ranging from 10 m at the top to 530 m at the bottom. Temperature is the only tracer variable (no salinity) and a linear equation of state is used. Scale dependent Laplacian viscosity is applied, and no explicit horizontal diffusion is imposed. An isopycnal diffusivity of $300\,m^2\,s^{-1}$ is used with the Gent and Mcwilliams (1990) parametrization. Advection scheme 7 in MITgcm (Daru and Tenaud, 2004) is used for temperature, to minimize numerical diffusion.

This configuration is a highly idealized representation of the Atlantic Ocean with the ACC at its Se. The model is forced at the surface by fixed winds and by restoring temperature to a fixed profile on a monthly time scale. The standard wind stress profile

OSD
10, 2461–2479, 2013

and restoring temperature are shown in Fig. 3 and the different forcings and diffusivities used are summarized in Table 1. In all experiments the vertical diffusivity in the interior, listed in the last column of Table 1, increases in the upper 50 m to $5.0 \times 10^{-3}\,m^2\,s^{-1}$. All the experiments are performed by spinning up the model from rest for 5000 yr with an asynchronous time stepping, to establish a preliminary stratification. The use of an asynchronous time stepping, necessary to reduce computational time, unfortunately prevents a detailed analysis of the equilibration mechanism. The model is then run for 500 yr with the same time step for momentum and temperature, and the results in the next section are derived from the last 50 yr the simulation. A residual trend is observed for deep ocean temperature, but not for the quantities considered here.

4 Results

Zonally averaged potential temperature in run A is shown in Fig. 4 (top). Taking the southern temperature (5.7 °C for run A) as the lower boundary of the pycnocline, the pycnocline depth is close to 500 m. It is shallower compared to the real pycnocline, and the MOC is rather shallow too. This is due to the periodic channel being only 1/3 as wide as the real ACC, with a consequently smaller Ekman flow and shallower pycnocline and a weaker overturning rate connecting the ACC to the basin (Allison et al., 2010). In Fig. 4, the overall stratification discussed in Sect. 2 can be observed. In particular, it is clear from the lower panel that the temperature and velocity structure at the Ne of the pycnocline is generally consistent with the two-layer idealization of Fig. 1, and that the southern temperature can indeed identify the lower boundary of the pycnocline. This general structure is similar for all simulations, and the depth of Ψ in the mid latitudes is well correlated to the maximum depth reached by b_S in all simulations.

To evaluate the skill of the scalings, the temperature differences entering the scalings have to be chosen. The northern temperature, b_N, is defined as the zonal average surface temperature at the northernmost latitude, west of 15° E (see Fig. 2). The results

OSD
10, 2461–2479, 2013

are not very sensitive to this choice; this particular definition is used since the highest surface densities are reached therein in the model. The southern temperature, b_S, is defined as the zonal mean surface temperature at a latitude of 50° S, at the Ne of the periodic channel. The southern temperature may be estimated also by averaging over a latitudinal interval, but by taking the zonal average at a single latitude we stress the fact the MOC strength is governed by the properties in a narrow region, at the bottom of the pycnocline and at its outcropping latitude. The depth scale can be measured as the maximum depth reached by the southern temperature on the eastern boundary in the NH.

In the simulations, a large part of the overturning is confined at the Ne of the basin, at least for the low–diffusivity simulations (as run A in Fig. 4). A large part of the water sinking at the northern boundary upwells already in the center of the subpolar gyre. This is probably an artifact of the low-resolution model used here, that has a too broad and weak rim current in the subpolar gyre, not substantially warmer than the interior. Being interested in the basin scale MOC, we measure Ψ by the maximum south of the latitude where b_S reaches its maximum depth on the eastern boundary, before outcropping in the NH. In practice, this means measuring the maximum at the subtropical–subpolar gyres boundary (red cross in the top panel of Fig. 4). Other measures of Ψ can in fact be used, including the global MOC maximum with similar conclusions; the one used here gives the best results.

It is interesting to consider first the prediction of the MOC strength using the geostrophic scaling (Eq. 3), based on Δb_{EW} (Fig. 5a). The scaling plotted is in this case the maximum of the right hand side of Eq. (3) in the NH, showing a high correlation (0.91) with Ψ. This is true particularly, but by no means exclusively, for the simulations with lower diffusivity (blue color in the figure). The MOC in this model is therefore certainly in geostrophic balance.

A step forward is made evaluating the MOC strength predicted by the scaling (Eq. 4), based on Δb_{SN}. (Fig. 5b). Also this scaling, computed in a completely independent way from the other, gives a very good estimate of Ψ in the simulations considered

OSD
10, 2461–2479, 2013

(correlation 0.88). The agreement is again particularly good for the set of simulations with the lowest vertical diffusivity. Measuring the buoyancy difference between the Ne of the basin and the Ne of the periodic channel is an effective way to estimate the MOC strength, since it is in fact a way to estimate the east–west buoyancy difference setting the MOC strength by thermal wind in the NH. This is confirmed by the results in Fig. 5c, demonstrating the high correlation (0.96) between the two scalings, one based on the east–west and the other on the north–south buoyancy difference. This holds to a large extent for the cases with larger vertical diffusivity too (Fig. 5, green and red points).

5 Discussion and conclusions

The results presented here can be seen as an extension of those in Johnson and Marshall (2002) (cf. Eq. 1), with an important new element: the lightest buoyancy involved in the scaling is not an average over the whole pycnocline, but rather the value at its lower boundary. A two-layer system, however, seems to be an oversimplification to represent the processes determining the MOC strength, and if a connection has to be made between meridional buoyancy gradient and vertical stratification.

This is evident considering in particular the results for experiments A and F, which differ only for the restoring temperature in the tropical region. The zonally averaged temperature structure in the two simulations is markedly different (not shown), with both a warmer pycnocline and a warmer interior in run F (the configuration with warmer tropical surface temperature). However, the two simulations have very similar MOC strength, the pycnocline depth and the temperature at the base of the pycnocline being virtually the same, since diffusivity plays a secondary role. The difference between the two simulations is in the northern temperature alone, higher in run F since the water flowing northward from the pycnocline is warmer; this difference is responsible for the slightly lower MOC strength in run F. Measuring the southern temperature entering the scaling over a larger area, e.g. averaging over the tropical ocean as in Levermann and Fürst (2010) would clearly fail to predict the correct MOC strength. The scaling

OSD
10, 2461–2479, 2013

Eq. (4) is less successful for cases H and K (equivalent to A and F respectively) due to the stronger impact of surface boundary conditions in the tropics using a higher vertical diffusivity of $5 \times 10^{-5}\,m^2\,s^{-1}$. For these higher vertical diffusivity values, vertical propagation of surface anomalies breaks, at least to some extent, the link between the periodic channel in the south and the Ne of the basin, even if geostrophy still gives a good prediction of Ψ (Fig. 5a). This points out the importance of the knowledge of the geographic distribution of vertical diffusivity for correctly predicting the MOC rate; a high diffusivity in the ACC, or in a second basin connected via the ACC, would influence b_S without changing the topology connecting b_S to b_E.

Our hypothesis can be linked to the adiabatic overturning paradigm of Samelson (2004) and Wolfe and Cessi (2011). In the vanishing vertical diffusivity limit, Wolfe and Cessi (2010) argued that the scaling (Eq. 3) can be rewritten using, instead of Δb_{EW}, the buoyancy interval Δb_c. The latter is measured by the surface density classes shared between the periodic channel and the dense water formation regions in the North Atlantic. We suggest here that this holds also for finite vertical diffusivity, since stratification in the semi–enclosed basin remains coupled to the one in the periodic channel even for finite vertical diffusivity.

The hypothesis we discussed may in particular explain why the SH, and in particular the Antarctic Intermediate Water formation regions, exerts a strong control on the dynamics of the MOC in numerical models, as discussed in Cimatoribus et al. (2012).

Acknowledgements. A. A. Cimatoribus would like to thank Will de Ruijter, David Marshall and Leo Maas for their insightful and useful comments at various stages of this work.

References

Allison, L. C., Johnson, H. L., Marshall, D. P., and Munday, D. R.: Where do winds drive the Antarctic Circumpolar Current?, Geophys. Res. Lett., 37, L12605, doi:10.1029/2010GL043355, 2010. 2467

Cessi, P. and Wolfe, C. L.: Eddy–driven buoyancy gradients on eastern boundaries and their role in the thermocline, J. Phys. Oceanogr., 39, 1595–1614, 2009. 2464
Cimatoribus, A., Drijfhout, S., den Toom, M., and Dijkstra, H.: Sensitivity of the Atlantic meridional overturning circulation to South Atlantic freshwater anomalies, Clim. Dynam., 39, 2291–2306, 2012. 2470
Cunningham, S. A., Kanzow, T., Rayner, D., Baringer, M. O., Johns, W. E., Marotzke, J., Longworth, H. R., Grant, E. M., Hirschi, J. J.-M., Beal, L. M., Meinen, C. S., and Bryden, H. L.: Temporal variability of the Atlantic Meridional Overturning Circulation at 26.5° N, Science, 317, 935–938, 2007. 2464
Daru, V. and Tenaud, C.: High order one–step monotonicity–preserving schemes for unsteady compressible flow calculations, J. Comput. Phys., 193, 563–594, 2004. 2466
De Boer, A. M., Gnanadesikan, A., Edwards, N. R., and Watson, A. J.: Meridional density gradients do not control the Atlantic Overturning Circulation, J. Phys. Oceanogr., 40, 368–380, 2010. 2463
Den Toom, M. and Dijkstra, H. A.: Scaling of the strength of the meridional overturning with vertical diffusivity in an idealized global geometry, Tellus A, 63, 354–370, 2011. 2462
Dijkstra, H. A.: Scaling of the Atlantic meridional overturning circulation in a global ocean model, Tellus A, 60, 749–760, 2008. 2463
Gent, P. R. and Mcwilliams, J. C.: Isopycnal mixing in ocean circulation models, J. Phys. Oceanogr., 20, 150–155, 1990. 2466
Gnanadesikan, A.: A simple predictive model for the structure of the oceanic pycnocline, Science, 283, 2077–2079, 1999. 2463
Griesel, A. and Maqueda, M. A. M.: The relation of meridional pressure gradients to North Atlantic deep water volume transport in an ocean general circulation model, Clim. Dynam., 26, 781–799, 2006. 2464
Hautala, S. L., Roemmich, D. H., and Schmilz, W. J.: Is the North Pacific in Sverdrup balance along 24° N?, J. Geophys. Res.-Oceans, 99, 16041–16052, 1994. 2464
Hughes, G. O. and Griffiths, R. W.: Horizontal convection, Annu. Rev. Fluid Mech., 40, 185–208, 2008. 2462
Johnson, H. L. and Marshall, D. P.: A theory for the surface Atlantic response to thermohaline variability, J. Phys. Oceanogr., 32, 1121–1132, 2002. 2463, 2469, 2475

OSD
10, 2461–2479, 2013

Johnson, H. L., Marshall, D. P., and Sproson, D. A. J.: Reconciling theories of a mechanically driven meridional overturning circulation with thermohaline forcing and multiple equilibria, Clim. Dynam., 29, 821–836, 2007. 2463

Levermann, A. and Fürst, J. J.: Atlantic pycnocline theory scrutinized using a coupled climate model, Geophys. Res. Lett., 37, L14602, doi:10.1029/2010GL044180, 2010. 2463, 2469

Marotzke, J.: Boundary mixing and the dynamics of three–dimensional thermohaline circulations, J. Phys. Oceanogr., 27, 1713–1728, 1997. 2463

Marotzke, J. and Klinger, B. A.: The dynamics of equatorially asymmetric thermohaline circulations, J. Phys. Oceanogr., 30, 955–970, 2000. 2463, 2464

Marshall, D. P. and Johnson, H. L.: Propagation of meridional circulation anomalies along western and eastern boundaries, J. Phys. Oceanogr., 43, 2699–2717, doi:10.1175/JPO-D-13-0134.1, 2013. 2466

Marshall, D. P. and Pillar, H. R.: Momentum balance of the wind–driven and Meridional Overturning Circulation, J. Phys. Oceanogr., 41, 960–978, 2011. 2464

Marshall, J., Adcroft, A., Hill, C., Perelman, L., and Heisey, C.: A finite–volume, incompressible Navier–Stokes model for studies of the ocean on parallel computers, J. Geophys. Res., 102, 5753–5766, 1997. 2466

Park, Y.-G. and Bryan, K.: Comparison of thermally driven circulations from a depth-coordinate model and an isopycnal-layer model, Part I: Scaling-law sensitivity to vertical diffusivity, J. Phys. Oceanogr., 30, 590–605, 2000. 2463

Samelson, R. M.: Simple mechanistic models of middepth meridional overturning, J. Phys. Oceanogr., 34, 2096–2103, 2004. 2470

Sijp, W. P., Gregory, J. M., Tailleux, R., and Spence, P.: The key role of the western boundary in linking the AMOC strength to the north–south pressure gradient., J. Phys. Oceanogr., 42, 628–643, doi:10.1175/JPO-D-11-0113.1, 2012. 2464

Stommel, H.: Thermohaline convection with two stable regimes of flow, Tellus, 13, 224–230, 1961. 2462, 2463

Tailleux, R.: Available potential energy and exergy in stratified fluids, Annu. Rev. Fluid Mech., 45, 35–58, 2013. 2464

Talley, L.: Closure of the global overturning circulation through the Indian, Pacific, and southern oceans: schematics and Transports, Oceanography, 26, 80–97, 2013. 2466

OSD
10, 2461–2479, 2013

Thorpe, R. B., Gregory, J. M., Johns, T. C., Wood, R. A., and Mitchell, J. F. B.: Mechanisms determining the Atlantic thermohaline circulation response to greenhouse gas forcing in a non-flux-adjusted coupled climate model, J. Climate, 14, 3102–3116, 2001. 2463

Vallis, G. K.: Large–scale circulation and production of stratification: effects of wind, geometry, and diffusion, J. Phys. Oceanogr., 30, 933–954, 2000. 2465

Wang, C., Dong, S., and Munoz, E.: Seawater density variations in the North Atlantic and the Atlantic meridional overturning circulation, Clim. Dynam., 34, 953–968, 2010. 2463

Weijer, W., De Ruijter, W. P., Sterl, A., and Drijfhout, S. S.: Response of the Atlantic overturning circulation to South Atlantic sources of buoyancy, Global Planet. Change, 34, 293–311, 2002. 2463, 2464

Wolfe, C. L. and Cessi, P.: What sets the strength of the middepth stratification and overturning circulation in Eddying ocean models?, J. Phys. Oceanogr., 40, 1520–1538, 2010. 2470

Wolfe, C. L. and Cessi, P.: The Adiabatic Pole–to–Pole Overturning Circulation, J. Phys. Oceanogr., 41, 1795–1810, 2011. 2470

Wunsch, C.: The decadal mean ocean circulation and Sverdrup balance, J. Mar. Res., 69, 417–434, 2011. 2464

OSD
10, 2461–2479, 2013

Table 1. Summary of the numerical experiments performed. From left to right, the table reports the name of the experiment, the maximum wind stress in the SH (westerlies), the restoring temperature at the Ne of the basin, the maximum restoring temperature (at or close to the equator), the restoring temperature at the Se of the basin and the vertical diffusivity in the ocean interior. See also Fig. 3.

Name	SH wind [Pa]	T north [°C]	T max [°C]	T south [°C]	Vert. diff. [$m^2 s^{-1}$]
A	0.1	0.5	18.0	−0.5	1.0×10^{-5}
B	0.15	0.5	18.0	−0.5	1.0×10^{-5}
C	0.055	0.5	18.0	−0.5	1.0×10^{-5}
D	0.1	0.5	18.0	−1.5	1.0×10^{-5}
E	0.1	0.5	18.0	0.5	1.0×10^{-5}
F	0.1	0.5	21.0	−0.5	1.0×10^{-5}
G	0.2	0.5	18.0	−0.5	1.0×10^{-5}
H	0.1	0.5	18.0	−0.5	5.0×10^{-5}
I	0.1	0.5	18.0	−1.5	5.0×10^{-5}
J	0.055	0.5	18.0	−0.5	5.0×10^{-5}
K	0.1	0.5	21.0	−0.5	5.0×10^{-5}
L	0.2	0.5	18.0	−0.5	5.0×10^{-5}
M	0.1	0.5	18.0	−0.5	1.0×10^{-4}

OSD
10, 2461–2479, 2013

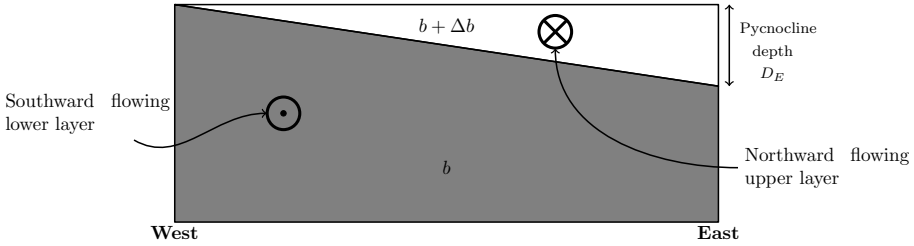

Fig. 1. Idealized view of the two layer model of Johnson and Marshall (2002). A zonal transect at the latitude where the pycnocline outcrops in the west is shown. In the upper (lower) layer the flow is northward (southward). The shear between the two layers is set by thermal wind balance.

OSD
10, 2461–2479, 2013

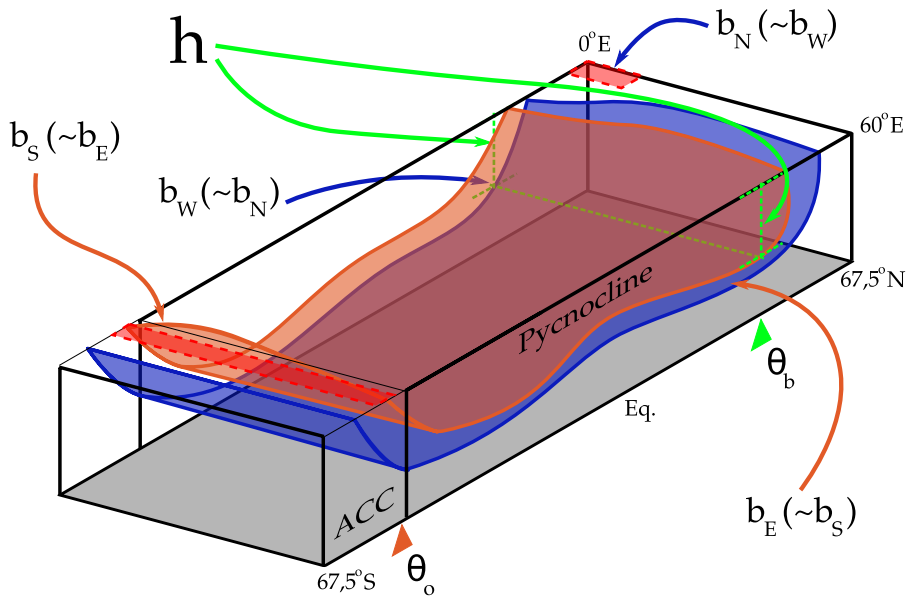

Fig. 2. Idealized perspective view of the two surfaces of constant buoyancy involved in the scaling, $b_N \sim b_W$ and $b_S \sim b_E$, in a closed basin with a periodic channel at its Se (ACC). The depth h and the latitude where the MOC reaches its maximum are shown by the green dashed lines. The green triangle and θ_b mark the latitude where b_S reaches its maximum depth at the eastern boundary. The brown triangle and θ_O mark the latitude where the pycnocline outcrops in the SH. The pycnocline, above the upper isopycnal drawn in the figure, is marked, as well as the periodic channel in the south, representing the ACC. The red dashed boxes mark the regions where the estimates of b_N and b_S are measured in the numerical model. The latitudes and longitudes in the drawing refer to the numerical model used.

OSD
10, 2461–2479, 2013

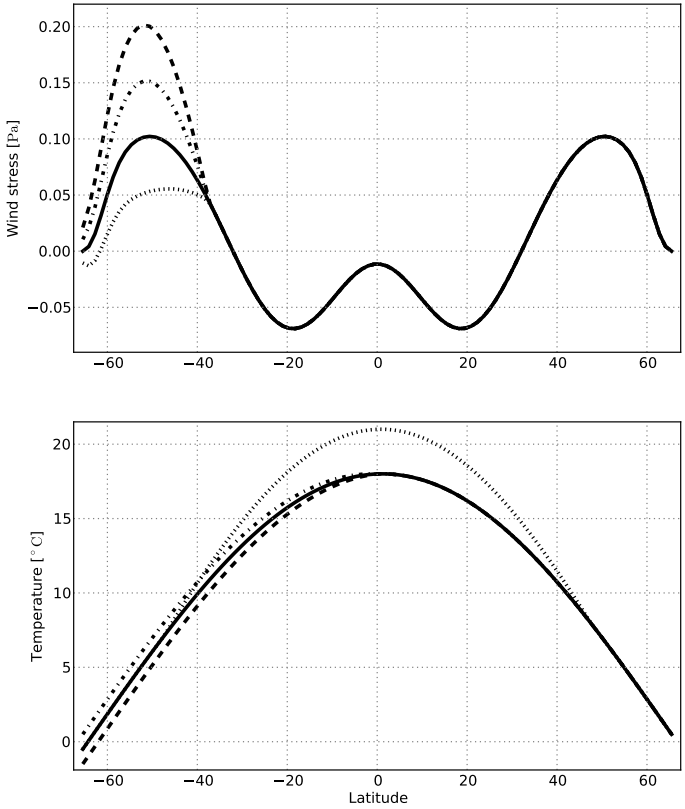

Fig. 3. Forcing profiles for wind stress (top) and temperature (bottom), the different line styles refer to different experiments (see text and Table 1). The strength of the SH westerlies alone is changed, while temperature is changed only over the SH or in the tropics and subtropics (dotted line, run F). As an example, full lines in both panels give the forcing of run A, the dashed dotted line for wind and full line for temperature gives the forcing for run B, etc.

OSD
10, 2461–2479, 2013

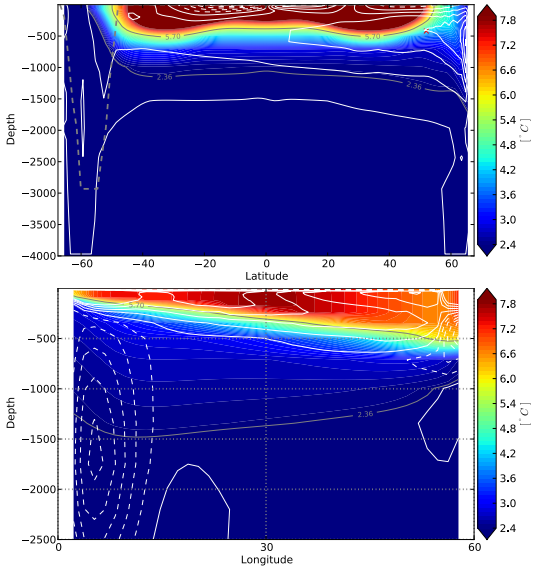

Fig. 4. The figure shows several fields from run A, computed as an average over years 5 450–5 500 of the simulation (the last 50 yr of the simulation). The upper panel shows zonally averaged fields, while the lower panel shows a zonal transect at 52° N, the latitude where b_S reaches its maximum depth on the eastern boundary (see text). The filled contours show in both panels the potential temperature, the two continuous gray lines show the isotherms of the "northern" and "southern" temperature used in the scaling, 2.36 °C and 5.7 °C respectively (see text). Upper panel: the white contours show the MOC streamfunction with a contour interval of 2 Sv, full contours being positive (zero included) and dashed contours being negative. The dashed gray line marks the depth of the periodic channel in the SH. The red cross marks the position of the MOC maximum used in the scaling (see text). Lower panel: the white contours show the meridional velocity every 0.002 m s^{-1}, with full contours being positive (starting at 0.001 m s^{-1}) and dashed contours being negative (starting at −0.001 m s^{-1}).

OSD
10, 2461–2479, 2013

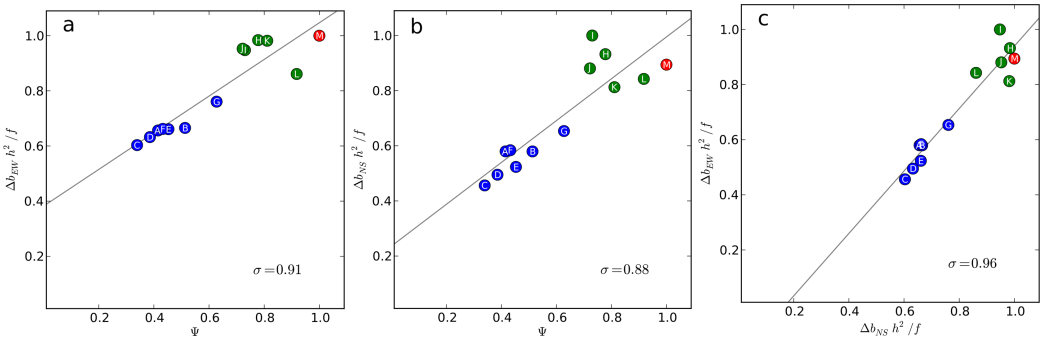

Fig. 5. The MOC strength (Ψ) predicted from the scalings $\Psi \sim (1/f)\Delta b_{\mathrm{EW}} h^2$ **(a)** and $\Psi \sim (1/f)\Delta b_{\mathrm{SN}} h^2$ **(b)** as a function of the measured MOC. The correlation between the two scalings is shown in **(c)**. Colors refer to the vertical diffusivity prescribed in the ocean interior: $1.0 \times 10^{-5}\,\mathrm{m^2\,s^{-1}}$ (blue), $5.0 \times 10^{-5}\,\mathrm{m^2\,s^{-1}}$ (green), $1.0 \times 10^{-4}\,\mathrm{m^2\,s^{-1}}$ (red). The MOC strength is measured by the maximum in the subtropical ocean (see text). The coordinates for the scatter plot are normalized to the maximum along each direction. The letters in the circles refer to the experiment names of Table 1. The gray lines are linear regressions through the data. The correlation between the data sets are reported in each panel.

OSD
10, 2461–2479, 2013